Crystal field splitting on D↔S transitions of atomic manganese isolated in solid krypton

O. Byrne, M. A. Collier, M. C. Ryan, and J. G. McCaffrey[a)]

Department of Chemistry, National University of Ireland, Maynooth, County Kildare, Ireland
(Submitted December 16, 2009)
Fiz. Nizk. Temp. **36**, 524–531 (May 2010)

Narrow excitation features present on the $[Ar]3d^64s^1a^6D_{(J=9/2-1/2)} \leftarrow [Ar]3d^54s^2a^6S_{1/2}$ transitions of manganese atoms isolated in solid Kr are analyzed within the framework of weak crystal field splitting. Use of the W_p optical lineshape function allowed identification of multiple zero-phonon lines for individual spin-orbit J states of the a $a^6D \leftarrow a^6S$ transition recorded with laser-induced excitation spectroscopy. Excellent agreement exists between the predicted crystal field splitting patterns for the J levels of the a^6D state isolated in the «red» tetravacancy site of solid Kr. The tetrahedral crystal field of the «red» trapping site splits $J>3/2$ levels of the a^6D_J and $a^4D_{7/2}$ states by approximately 30 cm^{-1}. This report represents the first definitive evidence of crystal field splitting, induced by the weak van der Waals interactions between a neutral metal atom and the rare gas atoms surrounding it in a well-defined solid-state site. © *2010 American Institute of Physics*. [doi:10.1063/1.3432260]

I. INTRODUCTION

In a series of recent papers, our group at Maynooth has reported the luminescence spectroscopy[1–3] of matrix-isolated atomic manganese and found that the site of isolation plays a very significant role in determining the emission linewidths and bandshapes. This effect was identified in the emission of $D \rightarrow S$ transitions where Mn atoms isolated in «red» sites[4] exhibited narrow, structured bands while atoms in «blue» sites exhibited broad, featureless emission strongly shifted from the gas phase position. The a^4D and a^6D states exhibiting this behaviour were produced, as indicated in Fig. 1, with excitation of the z^6P resonance at approximately 400 nm. In the absence of molecular dynamics calculations the identities of the sites producing the «red» and «blue» absorption bands are not known definitively. However, trends identified in the absorption and excitation spectra[5] of atomic manganese in a series of solid rare gases enabled us to attribute the «blue» and «red» features to single substitutional (SV) and tetra-vacancy (TV) sites respectively. Manganese atoms preferentially occupy the «red» (TV) site in solid Ar, the «blue» (SV) site dominates slightly in Kr while the «blue» site is the only thermally stable site occupied in Xe.

Laser-induced excitation spectra recorded[3] by monitoring «red» (TV) site emission features of Mn/Ar and Mn/Kr allowed identification of the five spin-orbit levels ($J=1/2$, $3/2$, $5/2$, $7/2$, and $9/2$) of the a^6D state. The laser excitation spectrum recorded for Mn/Kr monitoring the «red» site emission at 12 K is presented in the upper panel of Fig. 2. The sharp features at 17069, 17293, 17466, 17592, and 17662 cm^{-1} correspond to the J=9/2, 7/2, 5/2, 3/2, and 1/2 levels respectively but with a constant blue shift of about 17 cm^{-1} from the gas phase positions. This behavior indicates that the spin-orbit splitting of the a a^6D state in the gas phase is maintained for the Mn atom isolated in the TV site. However, it is quite evident in the spectra shown in Fig. 2 that numerous resolved features present in the Mn/Kr a^6D state excitation spectra have not been assigned yet.

In this contribution we analyze the origin of highly structured site-specific excitation and emission features present on the $D \rightarrow S$ transitions of atomic manganese in solid Kr.[2,3] The transitions examined are presented in Fig. 1. They occur between the $[Ar]3d^54s^2a^6S$ ground state and either a) the $[Ar]3d^64s^1$ a^6D state or b) the $[Ar]3d^64s^1$ a^4D state observed in excitation and emission respectively. Temperature dependent excitation spectra recorded for the $a^6D \leftarrow a^6S$ transitions are the subject of a detailed lineshape analysis which has allowed us to simulate the phonon structure on these transitions, but more importantly, has enabled identification of multiple zero-phonon lines (ZPL). The presence of multiple ZPLs on the individual a^6D_J spin-orbit levels for Mn atoms isolated in matrix sites of tetrahedral symmetry, represents the first definitive evidence of rare gas host

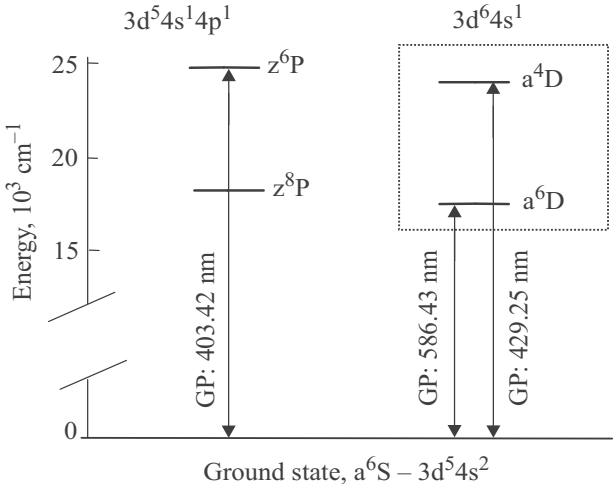

FIG. 1. An energy level diagram of the lowest energy states of gas phase atomic manganese. The fully allowed $z^6P_{5/2} \leftarrow a^6S_{5/2}$ transition occurring at 24788 cm^{-1} (403.42 nm) in the gas phase is indicated on the left. The area of the diagram shown in the dotted box, highlights the excited states that exist below the z^6P state which are accessible in relaxation occurring after $z^6P \leftarrow a^6S$ photoexcitation.

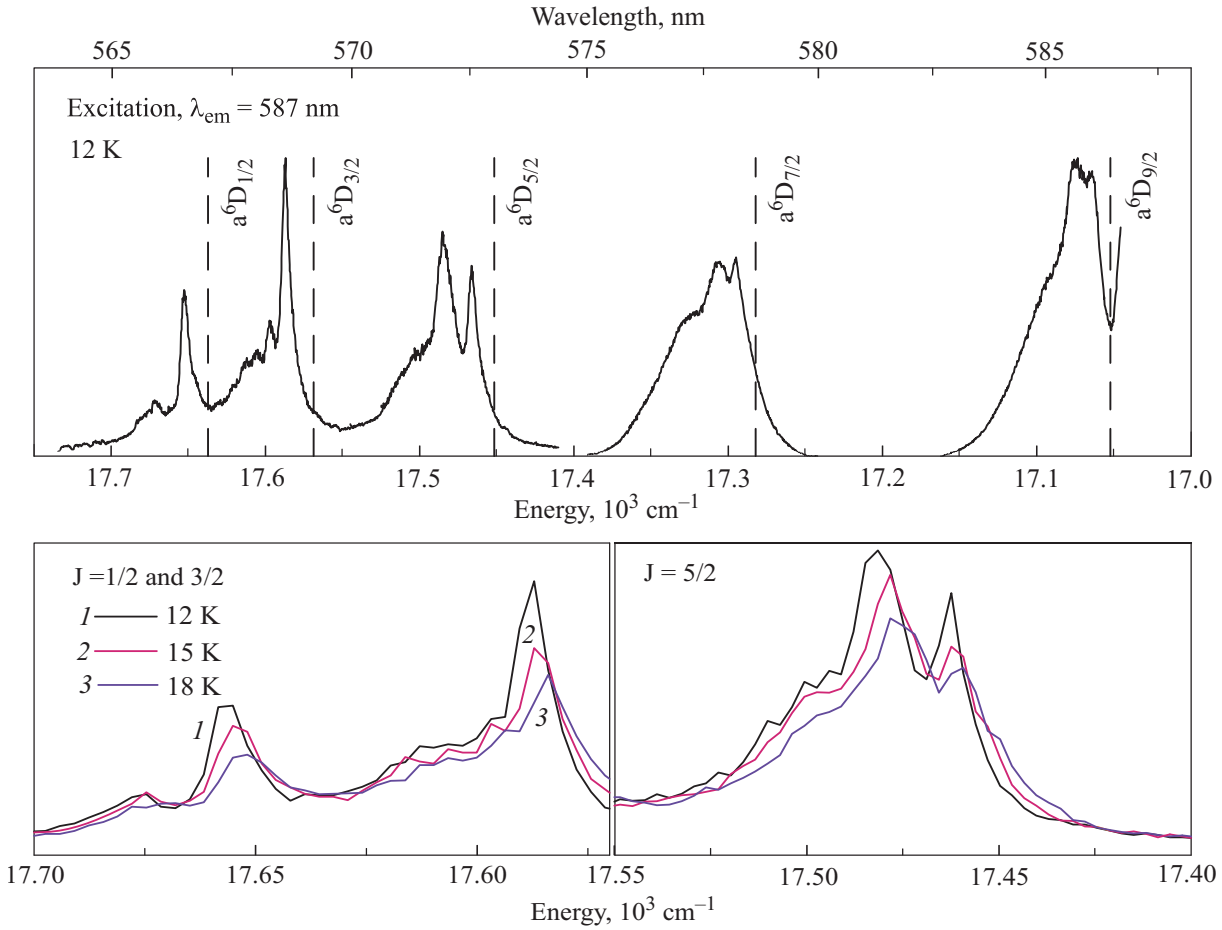

FIG. 2. High resolution laser excitation spectra recorded at 12 K in an annealed Mn/Kr sample. The spectra were recorded with Rhodamine 590 and Rhodamine 610 monitoring emission and 587 nm. The dashed vertical lines indicate the positions of the five gas phase $a^6D_J \leftrightarrow a^6S_{5/2}$ transitions to the spin-orbit levels of the a^6D_J state. The two panels shown on the bottom present the temperature dependence of the $J=1/2$, $3/2$, and $5/2$ spin-orbit levels.

inducing crystal field splitting on a metal atom.

This paper is structured as follows. Firstly, laser excitation spectra recorded at various temperatures are presented for the $a^6D \leftarrow a^6S$ transition of atomic Mn isolated in solid Kr. The lineshapes observed in excitation are simulated using the optical W_p function[7] from which the splitting patterns for the individual spin-orbit levels have been identified. Results of the excitation lineshape analyses are compared to predictions obtained from group theory for the effects of weak crystal fields on Mn D-state atoms isolated in sites of cubic (tetrahedral) symmetry. Finally, the crystal field interpretation is evaluated by comparison to the $a^4D_{7/2} \leftarrow a^6S$ emission spectra previously reported by the Maynooth Group.[1]

II. EXPERIMENTAL

The gas handling system and vacuum apparatus used in the preparation of Mn/RG matrix samples have been described in previous publications from our group.[8] The results reported in that study were recorded in the most dilute Mn/RG samples formed as evidenced by the absorption spectroscopy reported previously.[1] The experimental set-up used for recording excitation and emission spectra have been described in detail elsewhere.[3,8] Briefly, laser excitation spectra were recorded by scanning the output of a Nd:YAG pumped Quantel TDL90 dye laser in the region of the a^6D $-^6S$ transition at 586.43 nm. Rhodamine 590 was the dye used to cover the spectral range 555 to 585 nm, while Rhodamine 610 was used in the range 572 to 600 nm. The laser excitation spectra presented have not been corrected for the dye curves. Scans recorded with each dye are merged in the figures to provide complete coverage for the spectral ranges of interest. A 0.5 m (Acton Research Corporation, model ARC SP500i) monochromator fitted with three gratings and a photon counting (Hamamatsu R928-P) photomultiplier tube cooled to −20 °C were employed to monitor the emission from Mn/RG samples reported.

III. RESULTS AND ANALYSIS

A. Temperature dependent excitation of the Mn $a^6D \leftarrow a^6S$ transition

To determine the origin of the unassigned sharp features in the laser excitation spectra of the $a^6D \leftarrow a^6S$ transition, scans were recorded at higher temperatures. The lower panels in Fig. 2 present the Mn/Kr data recorded at 12, 15, and 18 K. Pronounced differences are observed in the intensities of the narrow a^6D_J, $J=5/2$, $3/2$, and $1/2$ bands. Most evident is the reduction in intensity of all narrow features with respect to broad underlying signals. This temperature dependence indicates that the narrow, low energy features are zero phonon lines. The unassigned features at 17309, 17292, and 17485 cm^{-1} also exhibit the temperature dependence of the ZPLs and accordingly are assigned as additional ZPLs on the

individual spin-orbit levels of the a^6D state. Thus the $J=7/2$ and $9/2$ levels both exhibit three ZPLs, the $5/2$ level has two ZPLs, while both the $3/2$ and $1/2$ levels have only one ZPL each.

B. Lineshape analysis of the Mn a $a^6D_J \leftarrow a^6S$ excitation spectra

To ascertain the true locations of the multiple ZPLs, lineshape analyses were conducted on the recorded excitation bands with the W_p optical function. This function accounts for the phonon-structure on an electronic transition and has been described in detail by Struck and Fonger.[7] It provides an analytic expression for the Franck-Condon intensity factors for displaced harmonic oscillators by assuming dominant coupling from a single phonon mode with a frequency $\hbar\omega$. The value of $\hbar\omega$ is taken to be the average of the fundamental frequencies for the ground and excited electronic states coupled in the transition. The key parameter in the W_p optical function fit is the strength of the electron-phonon coupling S, a term also known as the Huang-Rhys factor. An analytic expression for the W_p function is given in Eq. (1):

$$W_p = \exp\left(-S\frac{1+r}{1-r}\right) r^{-p/2} I_p\left(2S\frac{r^{1/2}}{1-r}\right) \tag{1}$$

in which $r=\exp(-\hbar\omega/kT)$, $I_p(x)$ is a modified Bessel function of variable order p, which at a given temperature T, has a fixed argument $\theta=2Sr^{1/2}/(1-r)$. To achieve numerical accuracy in simulating the very weak electron-phonon characteristics of the Mn/Kr excitation bands, the alternative sum form of the W_p function

$$W_p = \exp\left(-S\frac{1+r}{1-r}\right)\left(\frac{\theta}{2}\right)^p \sum_{k=0}^{\theta_m}\left(\frac{\theta^2}{4}\right)^k \frac{1}{k!\Gamma(p+k+1)} \tag{2}$$

was used in our analysis. The sum is carried out over the occupied phonon levels, k, and is truncated at θ_m, the next integer greater than $\theta+1$. The contribution of hot phonons ($-p$ terms) to the excitation is obtained by multiplying the W_p function in Eq. (2), with the appropriate Boltzmann factor *viz.* $W_{-p}=[\exp(-p\hbar\omega/kT)]W_p$. As will be shown later, even at 12 K, hot bands make a significant contribution to the overall excitation (or emission) bandshape when the phonon frequency is very small. The W_p lineshape analysis allows, as shown in our earlier work,[8] [8] identification of the band origin $\nu_{0,0}$, i.e., the zero phonon line (ZPL) and an assessment of the electron-phonon coupling strength S, for the electronic transition involved. The starting point for the W_p lineshape analysis is the selection of a value for the phonon frequency ($\hbar\omega$) required to transform the recorded spectrum into phonon units, p.

The lineshape analysis is greatly simplified by the pres-

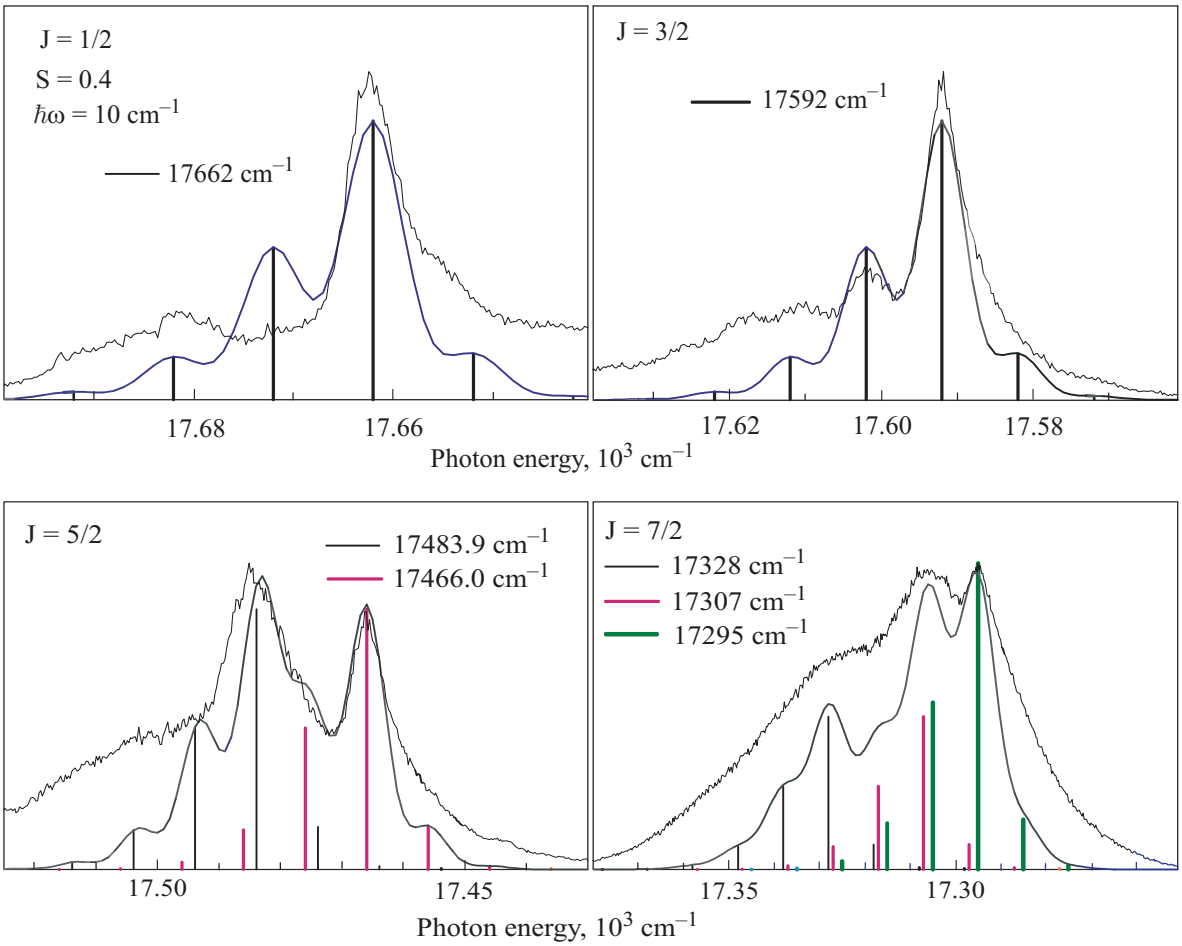

FIG. 3. Lineshape simulations obtained with the W_p optical function of the resolved features in the Mn/Kr excitation band profiles recorded for the a^6D_J, $J=1/2$, $3/2$, $5/2$ and $7/2 \leftarrow a^6S$ transitions at 12 K. The locations of the zero phonon lines are indicated in wavenumber units. The band profiles were [illegible]ing Gaussian line shapes (FWHM 6.6 cm^{-1}) for the W_p distributions described in the text.

ence of resolved hot bands in high temperature spectra since they provide a direct measurement of the magnitude of the phonon frequency $\hbar\omega$. Figure 3 presents details of the lineshape analyses completed for the $J=1/2$, $3/2$, $5/2$, and $7/2$ spin-orbit levels. The phonon frequency $\hbar\omega$ for $J=3/2$ was identified from the separation between the ZPL and the next resolved feature observed directly to the blue. A value of $\hbar\omega=10$ cm^{-1} was used thereafter for all fits. Initial estimates of the locations of the ZPLs were chosen as the narrow, most intense features in the spectra.

The band which yielded the simplest, most direct W_p fit was the excitation profile of the $J=3/2$ level. With an S value of 0.4, a single ZPL at 17592 cm^{-1} and with $\hbar\omega=10$ cm^{-1} all the resolved features in this excitation spectrum are satisfactorily reproduced including the occurrence of the hot band present even at 12 K. The solid grey line in Fig. 3 corresponds to the sum of the individual phonon intensities broadened to match the width of the resolved band at 17592 cm^{-1}. On the basis of the quality of this W_p fit it can be concluded that the structures present on the $J=3/2$ band arise from resolved phonon features occurring for an S value of 0.4. This is a small S value, indicating weak electron-phonon coupling.

A similar fit, using a single ZPL at 17662 cm^{-1} with identical S and $\hbar\omega$ values to $J=3/2$, was conducted for the $J=1/2$ level. The discrepancy which appears to exist in the W_p fit of this level, where the $p=1$ phonon level at 17672 cm^{-1} in the simulated lineshape is substantially overestimated, is an artifact that arises due to competitive absorption at 566 nm. This effect is evidenced by the asymmetric bandshape of the ZPL at 17662 cm^{-1} and possibly is produced by a vibrational band[9] of Mn_2 in this region.

Adequate fits were obtained for the $J=5/2$ level with two ZPLs located at 17484 and 17466 cm^{-1}. For the $J=7/2$ level, a satisfactory fit was obtained with three ZPLs at 17328, 17307, and 17295 cm^{-1}. The use of three ZPLs at 17100, 17081, and 17067 cm^{-1} accounted very well for the overall bandshape of the $J=9/2$ level as indicated on the left in Fig. 4. The reason for the poor resolution of this band compared to the other J values, arises from the fact that it was recorded by monitoring off-resonance emission at 587 nm to the red of the band maximum. In all of these fits a single phonon frequency of 10 cm^{-1} was used and S values of 0.4 were used throughout.

The results of all the W_p lineshape fits are collected in Table I. The presence of multiple ZPLs for individual spin-orbit levels of the a^6D state of Mn isolated in «red» TV sites in solid Kr can only be rationalized in terms of a crystal field splitting induced by the TV site occupied. With a knowledge that this site has tetrahedral symmetry, an evaluation of the effects of this field on both the term symbols and spin-orbit levels will be presented in the following section.

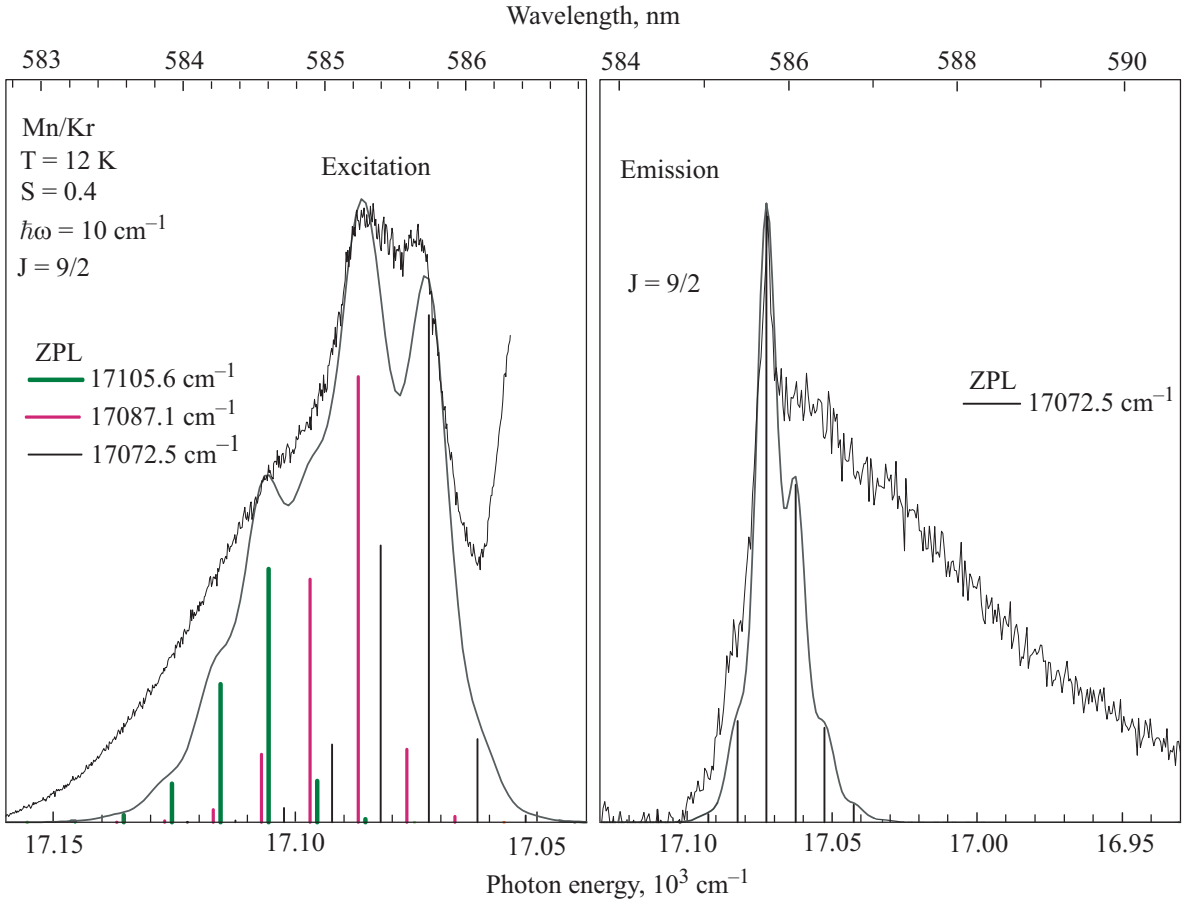

FIG. 4. Lineshape simulations, obtained at 12 K with the W_p optical function of the resolved features in the $J=9/2$ level, are shown on the left for excitation and on the right for emission. From the type of resolved structure present on the high energy portion of the emission, it would appear that only the lowest energy CF level contributes to the recorded profile. The simulation with a single ZPL accounts for this portion of the recorded emission but not the featureless ut to 590 nm.

TABLE I. Results of lineshape simulations of the Mn($a^6D_J \leftarrow a^6S$)/Kr excitation and Mn($a^4D_{7/2} \rightarrow a^6S$)/Kr and Ar emissionspectra using the W_p optical function as described in the text. The W_p fit parameters $\nu_{0,0}$ and $\hbar\omega$ are presented in wavenumber, cm^{-1} units while the Huang Rhys factor S, is unitless. Crystal field splitting (CFS) of matrix-isolated atomic manganese is identified as the difference between adjacent zero-phonon lines for a given spinorbitstate

Mn(a^6D_J)/Kr				
J	S	ZPL, cm^{-1}	CFS	$\hbar\omega$, cm^{-1}
1/2	0.4	17662	—	10
3/2	0.4	17592	—	10
5/2	0.4	17484	—	—
		17466	18	10
7/2	0.4	17295	—	—
		17307	12	10
		17328	21	—
9/2	0.4	17072.5	—	—
		17087.1	14.6	10
		17105.6	18.5	—
Mn($a^4D_{7/2}$)/RG				
Kr	0.4	23328	—	—
		23342	14	10
		23374	32	—
Ar	0.45	23352	—	—
		23358	6	12
		23388	30	—

C. Crystal field analysis

The absorption and excitation spectroscopy of atomic Mn reported by the Maynooth Group has allowed the identification of the most probable site occupancy of ground, a^6S, state manganese atoms in Ar, Kr and Xe.[5] These assignments were based on deposition site preferences evident in absorption spectra and the linear dependence found in matrix-shifts versus host polarizability plots. A comparison of the matrix luminescence of atomic magnesium (Mg/RG) with the manganese systems reinforced the site assignments made. It was concluded that the «red» sites present in solid Ar and Kr correspond to Mn atoms isolated in tetra-vacancy[3] sites (TV) of tetrahedral symmetry. The narrow line transitions to the a^6D state are only reported for Mn atoms occupying the TV site in Ar and Kr. As such, the crystal field analysis is applied to the a^6D state in a tetrahedral field generated by the tetravacancy site.

The magnitude of the crystal field splitting depends on the interplay of two factors; a) that electrons in the metal experience inter-electronic repulsions and b) the metal electrons are repelled by the electron density of the ligand (Lewis base). Thus, crystal field splitting can be approached from one of two extreme conditions. The first is the strong field limit in which the ligand-metal electron repulsions are larger than the inter-electronic repulsions (i.e., the ligands are strong Lewis bases). The second is the weak field limit where the repulsions between the metal electrons and the electron density of the ligands is small compared to inter-electronic repulsions. Both approaches involve use of the LS (also known as Russell-Saunders) coupling scheme. The LS coupling scheme assumes that the quantum numbers L and S can be dealt with separately and combine vectorially to give $J=L+S$, the spin-orbit levels. When S and J have half-integer values, as is the case for neutral atomic manganese, double groups devised by Bethe must be used to obtain representations for the spin-orbit levels. Briefly, the double groups[10] are generated from normal point groups by considering rotation by 2π as an independent symmetry operation, labelled R. Direct products of spatial and spin representations of double groups (denoted ') can be obtained in the same way as the usual symmetry groups and decomposed as sums of irreducible representations using the reduction formula.

The crystal field experienced by the Mn[Ar]$3d^64s^1a^6D$ state in the tetrahedral site symmetry (T_d) can be considered from the two extremes of either 1) The «strong field», where spin-orbit coupling is small or 2) The «weak field» where spin-orbit coupling is more important. In the strong field case the spatial $^6T_2$ and $^6E_1$ term symbols are derived from the ^6D state and spin-orbit coupling is considered a perturbation of the two ($^6T_2$ and $^6E_1$) spatial terms. In a weak crystal field, the effect of spin-orbit coupling is much greater than that of the crystal field causing a perturbation of the individual spin orbit levels, namely, $^6D_{1/2}$, $^6D_{3/2}$, $^6D_{5/2}$, $^6D_{7/2}$, and $^6D_{9/2}$.

1. Strong field

The strong crystal field case begins with the spatial $^6T_2$ and $^6E_1$ terms which arise for a ^6D term in a T_d field, that is by considering only the effect of the T_d field on the orbital quantum number, L. Here $S=5/2$, yielding the T_d' double group representation $\Gamma_{(S=5/2)}=\Gamma_7+\Gamma_8$ for the spin. The spatial term $^6E_1$ is Γ_3 while $^6T_2$ is Γ_5 in the T_d' field using Bethe notation. The effect of spin-orbit coupling on the spatial terms is obtained by taking direct products of the representation for the four combinations of $\Gamma_7+\Gamma_8(S=5/2)$ and $\Gamma_3+\Gamma_5(E_1+T_2)$. When the resulting representations are reduced, four energetically distinct spin-orbit levels ($\Gamma_6+\Gamma_7+2\Gamma_8$) emerge from the $^6E_1$ (T_d) term and six levels ($2\Gamma_6+\Gamma_7+3\Gamma_8$) from the $^6T_2$ in a strong crystal field. The effect of spin-orbit coupling on the pure crystal field terms are shown on the left side of Fig. 5. The energy of the $^6E_1$ term is lower than that for the [Ar]$3d^64s^1$ configuration of atomic Mn in a T_d crystal field.

2. Weak field

At the other extreme, where there is zero crystal field only SO coupling is present and the unsplit gas phase J levels of the a^6D_J state (with $J=1/2$, $3/2$, $5/2$, $7/2$, and $9/2$) would be observed in the solid matrix. As the crystal field strength is increased each of the J levels is then subject to perturbation by the T_d' field. In this case the spin-orbit levels (J) are treated individually and the total representation for each J is determined and decomposed using the T_d' character table yielding the effects of the weak CF on the individual SO levels, J. For example, the $J=5/2$ level is split by the tetrahedral field to give two spin-orbit states Γ_7 and Γ_8. The $J=7/2$ level splits into three spin-orbit states Γ_6, Γ_7, and Γ_8 while the $J=9/2$ level similarly splits to give three spin-orbit states Γ_6 and $2\Gamma_8$. These operations are shown on the right side of Fig. 5 for the a^6D state of Mn in a T_d crystal field. In contrast the $J=1/2(\Gamma_6)$ and $J=3/2(\Gamma_8)$ levels are not split by the crystal field.

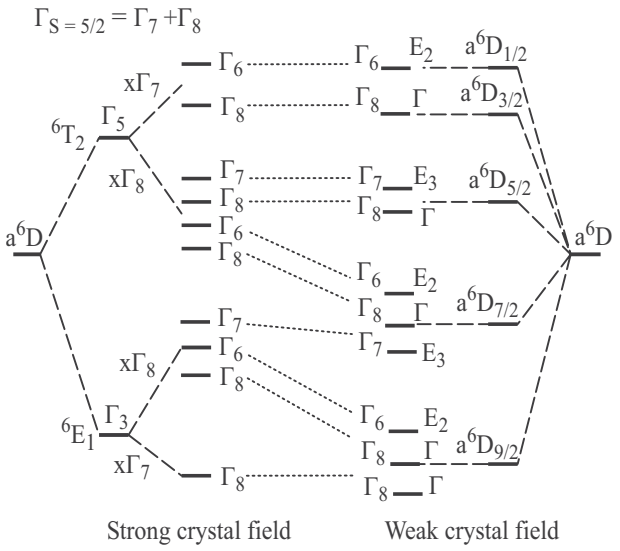

FIG. 5. A correlation diagram establishing the effect of a weak crystal field (CF) on the spin-orbit levels of the a ^6D_J state of atomic manganese isolated in a matrix site of tetrahedral symmetry (T_d').

The same number and type of spin-orbit levels are necessarily obtained whether one starts with the strong crystal field $^6E_1$ and $^6T_2$ terms or the weak field SO levels case just presented. This allows one to develop a correlation diagram spanning the intermediate field between the zero field a ^6D_J spin-orbit states and the strong crystal field states $^6E_1$ and $^6T_2$. Such a correlation diagram is shown in Fig. 5. To simplify the diagram, none of the states are shown to cross, although states of different double group symmetries may cross. Additionally, states of the same double group symmetry will undergo configuration interaction and avoid each other.

Experimentally the observation of distinct SO levels with multiple ZPLs in the matrix spectra for the a^6D_J state, clearly establishes that the SO coupling dominates and the crystal field interaction will act only to perturb the SO levels. Inspection of the right hand side of the correlation diagram shown in Fig. 5, reveals that a weak T_d field splits the J levels of the a^6D state as follows: $J=1/2 \Rightarrow E_2(\Gamma_6)$, $J=3/2 \Rightarrow G(\Gamma_8)$, $J=5/2 \Rightarrow G(\Gamma_8)+E_3(\Gamma_7)$, $J=7/2 \Rightarrow G(\Gamma_8)+E_3(\Gamma_7)+E_2(\Gamma_6)$ while $J=9/2 \Rightarrow G(\Gamma_8)+G(\Gamma_8)+E_2(\Gamma_6)$. The degeneracies of the double group irreducible representations are more evident when given in the alternative Mulliken notation, G and E. Thus the $J=7/2$ level will produce three energetically distinct CF levels G, E_3, and E_2 [Γ_8, Γ_7, and Γ_6] with degeneracies of 4, 2, and 2, respectively.

IV. DISCUSSION

The correlation diagram generated by considering the interaction of the a^6D state of atomic Mn in both strong and weak tetrahedral fields has allowed the prediction of the effect of a weak crystal field interaction in a TV site. Inspec-

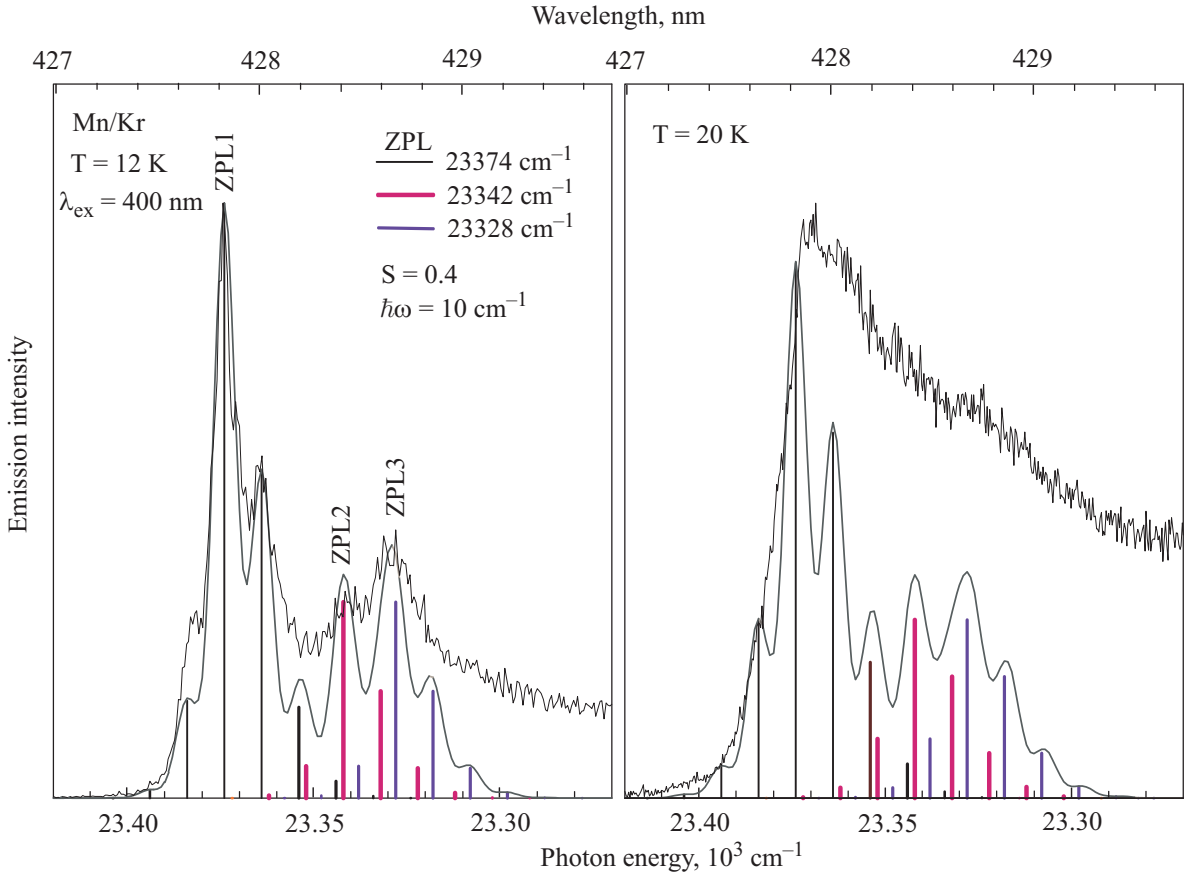

FIG. 6. High-resolution emission spectra recorded at 12 and 20 K with pulsed laser excitation of the thermally stable, «red», tetravacancy site occupied by atomic Mn in solid Krypton at 400 nm. Simulations of the resolved emission features were generated with the W_p line shape functions for 12 and 20 K. The locations of the zero phonon lines are indicated as ZPL1, ZPL2, and ZPL3, these values are shown in wavenumber units. The emission band profiles were ...ing Gaussian line shapes (FWHM 6.6 cm^{-1}) for the distributions and summing the three W_p distributions.

tion of Fig. 5, shows the $J=7/2$ and $9/2$ levels are each predicted to split into three weak field states. This is in agreement with the lineshape analysis presented in Figs. 3 and 4 where three ZPLs were located for both of these levels. The three ZPLs identified can now be assigned to direct excitation of each of the three Γ_is. Furthermore, no splitting is predicted on the $J=1/2$ and $3/2$ SO levels as they evolve into the weak field as Γ_6 and Γ_8, respectively. This is also in agreement with the lineshape analysis as one ZPL was located for each of the $a^6D_{1/2}$ and $a^6D_{3/2} \leftarrow a^6S_{5/2}$ excitation spectra.

In a previous analysis of the emission spectroscopy of Mn/Ar and Mn/Kr produced with excitation of the fully allowed $z^6P \leftarrow a^6S$ transition[1,2] crystal field splitting was tentatively assigned. Narrow emission features of the red (TV) site at approximately 428 nm were identified as having multiple ZPLs on the $a^4D_{7/2} \leftarrow a^6S_{5/2}$ transition of Mn in solid Ar and Kr. The original Mn/Kr lineshape analysis indicated the presence of two ZPLs but when the data are refit using information from the correlation diagram (Fig. 5) three ZPLs can be identified. The refit results of the Mn/Kr $a^4D_{7/2}$ emission are presented in Fig. 6 for two different temperatures. It is evident that the 12 K spectrum is well reproduced using three ZPLs. Two of the fitting parameters used, i.e., the electron–phonon coupling strength (S) and phonon frequency ($\hbar\omega$) were taken directly from the fits conducted for the a^6D_J excitation spectra. The fit only required identification of the band origins, $\nu_{0,0}$. i.e. the zero phonon line (ZPLs) positions. This approach is believed valid as both transitions involve the same excited state electronic configuration $3d^64s^1$ and occur within the same site of isolation.

In contrast to the a^6D excitation spectra simulated earlier, high-resolution $a^4D_{7/2} \rightarrow a^6S_{5/2}$ emission data are available for temperatures in excess of 12 K, as shown on the right in Fig. 6. The lineshape analysis with the W_p optical function can be checked easily. Figure 6 shows that the main features (shoulders) are reproduced by the fit but the intensity distribution in the red is not accounted for. The discrepancy is due to the presence of an overlapping emission feature from a thermally unstable site of Mn isolation. However, it is noteworthy that the emission may be fit successfully using the same parameters and a knowledge of the splitting pattern expected for the weak crystal field.

V. CONCLUSIONS

The W_p lineshape analyses conducted with small electron–phonon coupling strengths ($S=0.4$) account well for the resolved features present in the high-resolution excitation spectra. More significantly, the fits allow identification of several spectral features to multiple ZPLs for the $J=5/2$, $7/2$, and $9/2$ levels of the a^6D state and a single ZPL for both the $J=1/2$ and $3/2$ levels. The correlation diagram presenting the effect of varying crystal field strength on these spin-orbit states allowed assignment of each of the ZPLs as resulting from excitation to a particular spin-orbit state, Γ_i. The number of the ZPLs match the group theory predictions of the crystal field splitting of the individual J-levels. Overall, the multiple ZPLs identified in the lineshape fits are correctly predicted by the crystal field analysis which leads us to conclude that we have identified weak CFS on the spin-orbit levels of the a^6D state induced by the Kr atoms. Very narrow lines have been recorded previously on D states of matrix-isolated metal atoms, specifically the 1D state of Ca, studied by Bondybey,[11] Pellin *et al.*[12] on Cr and Mo, and Nixon and co-workers[13] on Fe, Co and Ni atoms. However, the W_p optical lineshape fits conducted in the present work present the most complete analysis of the existence of CFS. The extensive occurrence of hot bands, while useful in the initial fits, broaden the large J values making identification of the CF splitting and intensities difficult to definitively establish. This problem would be removed by working at lower temps than the 12 K limit available to us in the present study.

ACKNOWLEDGMENTS

This research was funded by the Irish Government Enterprise Ireland, SC/98/403 Basic Science research grant to whom MC gratefully acknowledges receipt of a Ph.D. studentship. The iCCD camera used in this work was acquired with the financial support of Science Foundation Ireland (SFI), Investigator grant 02/IN.1/B032. OB gratefully acknowledges the award of a Ph.D. studentship from Embark Initiative Irish Research Council for Science and Engineering (IRCSET) and a John & Pat Hume scholarship from N.U.I.—Maynooth.

[a]Email: john.mccaffrey@nuim.ie

[1]M. A. Collier and J. G. McCaffrey, J. Chem. Phys. **122**, 184507 (2005).
[2]M. A. Collier, Ph.D. Thesis, National University of Ireland Maynooth (2004); http://eprints.may.ie/archive/00000154/-01/MartinCollier,Thesis.pdf (Last accessed December 2009).
[3]M. A. Collier, M. C. Ryan, and J. G. McCaffrey, J. Chem. Phys. **123**, 044508 (2005).
[4]Use of the labels «blue» and «red» pertain to the locations of these sites in the absorption and excitation spectra recorded for the fully allowed $6P \leftarrow {}^6S$ resonance transitions.
[5]M. A. Collier and J. G. McCaffrey, J. Chem. Phys. **122**, 054503 (2005).
[6]N.I.S.T. Atomic Spectra Database; http://physics.nist.gov/-PhysRefData/ASD/ (Last accessed December 2009).
[7]C. W. Struck and W. H. Fonger, *Understanding Luminescence Spectra and Efficiency Using W_p and Related Functions*, Springer-Verlag, Berlin (1991).
[8]M. A. Collier and J. G. McCaffrey, J. Chem. Phys. **119**, 11878 (2003).
[9]A. D. Kirkwood, K. D. Bier, J. K. Thompson, T. L. Haslett, A. S. Huber, and M. Moskovits, J. Phys. Chem. **95**, 2644 (1991).
[10]B. S. Tsukerblat, *Group Theory in Chemistry and Spectroscopy*, Dover Press, New York (2006).
[11]V. E. Bondybey, J. Chem. Phys. **68**, 1308 (1977).
[12]M. J. Pellin, D. M. Gruen, T. Fischer, and T. Foosneas, J. Chem. Phys. **79**, 5871 (1983).
[13]T. A. Cellucci and E. R. Nixon, J. Phys. Chem. **89**, 1991 (1985) and references cited therein to earlier work. In particular M. T. McKenzie, Ph.D. *Thesis*, University of Pennsylvania (1983) (Unpublished Results).

This article was published in English in the original Russian journal. Reproduced here with stylistic changes by AIP.